



Hydrothermal-induced α -Fe₂O₃/graphene nanocomposite with ultrahigh capacitance for stabilized and enhanced supercapacitor electrodes

M. Jayashree¹ · M. Parthivarman² · S. Prabhakaran³

Received: 28 September 2018 / Revised: 21 December 2018 / Accepted: 28 December 2018 / Published online: 21 January 2019
© Springer-Verlag GmbH Germany, part of Springer Nature 2019

Abstract

Pure and Fe₂O₃/graphene (G) nanocomposite was prepared by novel one-step hydrothermal method. XRD results suggest that rhombohedral phase of α -Fe₂O₃ (hematite, space group: R3c), which are consistent with the values given in the standard card (JCPDS no. 33-0664). The N₂ adsorption–desorption results confirms that Fe₂O₃-G composite shows highest specific area (91 m² g⁻¹) and lower pore size of 10 nm compared with pristine Fe₂O₃ (surface area 76 m² g⁻¹ and pore size = 17 nm). The electrochemical measurement demonstrates that Fe₂O₃/G composite shows a specific capacitance as high as 315 F g⁻¹ at a discharge current density of 2 A g⁻¹. Even at the current density of 10 A g⁻¹, the specific capacitance is still as high as 185 F g⁻¹. After 2000 cycles, the capacity retention is still maintained at 98%. This result suggests that the Fe₂O₃/G nanocomposite is a promising electrode material for high-energy density supercapacitor application.

Keywords Graphene · Hydrothermal · Transmission electron microscope · Electrochemical · Supercapacitor

Introduction

With the improvement of the economy, environmental stress has been increasing, and it is extremely urgent to develop a new, low cost, environmentally friendly alternative energy source and energy storage system [1–4]. Supercapacitors are one of the most important as promising candidate material for energy storage because of their advantages such as high power density, excellent rate capacitance, and long cycle life [5–7]. Recently, a variety of transition-metal oxides, such as RuO₂, Co₃O₄, NiO, Fe₂O₃, Fe₃O₄, and MnO₂, have been studied for supercapacitor applications [8–10]. Iron oxides including Fe₃O₄ [11] and Fe₂O₃ [12] are considered as one of the most promising pseudocapacitor electrode materials due to its

abundance, low cost, environmental harmlessness, and high electrochemical performance. However, their serious disadvantages of limited electrode applications due to their poor electrical conductivities and the synthesis of these novel structures are quite complex and not easy to control. Another option that can improve the electrochemical performance is to combine α -Fe₂O₃ with other components with good conductivity to facilitate the electron transfer between the active materials and the current collector.

Recently, graphene is a unique single layer of carbon atoms tightly packed into a two-dimensional honeycomb sp² carbon lattice and has paying fabulous attention in energy storage devices as a result of its huge specific surface area, good chemical stability, and remarkable electrical conductivity [13]. Many literatures have reported that Fe₂O₃/graphene nanocomposites for supercapacitor applications. For example, Dewei Wang et al. [14] have prepared Nanostructured Fe₂O₃–graphene composite via facial hydrothermal method and prepared electrode material large specific capacitance (151.8 F g⁻¹ at 1 A g⁻¹), good rate capability (120 F g⁻¹ at 6 A g⁻¹), and excellent cyclability. Hang Zhang et al. [15] have prepared solvothermal-induced α -Fe₂O₃/graphene nanocomposite by hydrothermal method. The results showed that capacitances are admirable 2310 F g⁻¹ at 5 mV s⁻¹ and 615 F g⁻¹ at the amazing high current density of 100 A g⁻¹.

✉ M. Parthivarman
varmanphysics85@gmail.com

¹ Department of Physics, Vellalar College for Women, Erode, Tamil Nadu 638112, India

² PG and Research Department of Physics, Chikkaiah Naicker College, Erode, Tamil Nadu 638004, India

³ Centre for Crystal Growth, VIT University, Vellore, Tamil Nadu 632014, India

Attempt to further improvement in the electrochemical performance of these nanostructure materials, this work we have prepared Fe₂O₃/graphene nanocomposites via one step hydrothermal method and systematically investigated the thermal, structural, morphological, and electrochemical performances. The results showed that Fe₂O₃/G nanocomposites showed high specific capacitance, good rate capability, and excellent cyclability compared to pure Fe₂O₃. To the best of the author's knowledge, this is the first preliminary report about high performance electrochemical behavior of Fe₂O₃/G nanocomposite electrodes via a one step facile hydrothermal method.

Experimental procedure

Materials

Iron(III) nitrate [Fe(NO₃)₂], purity-99.97%, urea [CO(NH₂)₂], and liquid ammonium hydroxide solution (NH₄OH-purity-99.97%) were used as the precursor solutions for Fe₂O₃ nanostructures. All the chemicals used were of analytical grade, purchased from Merck, India, and without any further purification.

Preparation GO

Graphite oxide (GO) was synthesized from pristine graphite powder based on a modified Hummers method. In a typical process, 25 mg GO and 50 mL of water were ultrasonicated in a beaker for 90 min in order to fully exfoliate the graphite oxide to GO sheets. Finally, a homogeneous GO aqueous dispersion (0.5 mg mL⁻¹) was obtained.

Preparation Fe₂O₃/G nanocomposites

The Fe₂O₃/G nanocomposite was prepared by hydrothermal process using urea as fuel agent. In a typical experimental procedure, 0.1 M Fe(NO₃)₂ was dissolved in 50 mL distilled water under strong magnetic stirring until completely dissolved. Then, the prepared GO powder was mixed with the above solution. The ratio of Fe(NO₃)₂ and GO is 1:1. The urea was added in the above solution and stirred for 30 min. The ratio of Fe(NO₃)₂ and urea is 1:2. Then, 25 ml aqueous solution of NH₄OH was introduced into above aqueous solution to make the desired alkaline concentration until the pH value was attain 10. During this reaction, the drop rate was must be controlled to achieve the chemical homogeneity. Then, the solution was transferred into a Teflon lined stainless steel autoclave, which was sealed and maintained at 150 °C for 24 h. After completing the hydrothermal reaction, the mixture was centrifuged to get the precipitate out and washed with ethanol and distilled water and then dried in air in a laboratory hot air oven at 100 °C for 10 h. Pure Fe₂O₃ particles were also prepared in the same conditions without the presence of GO.

Characterization details

The thermal analysis was performed on SDT Q600 V8.3 Build 101 TGA system. The heating rate of 10 °C min⁻¹ in nitrogen flow (40 ml min⁻¹) and the weight of the sample taken in the experiment were around 5 mg. Identification of the crystalline phase and size of the Fe₂O₃/G nanocomposite was performed using powder X-ray diffraction (Bruker diffractometer) using the Cu K α wavelength of 1.5406 Å and operating at 35 kV and 30 mA. PXRD patterns were recorded in the range 20–80° at the scan rate of 0.50 s. Morphology and particle size of the prepared nanoparticles were studied, employing transmission electron microscope that was recorded with accelerating voltage of 200 kV. The elemental analysis of the samples was analyzed by EDS spectra (JEOL model JED-2300) operated at 15 kV. The Raman spectra of the samples were recorded using BRUKER RFS 27: stand-alone FT-Raman Spectrometer at a resolution of 0.2 cm⁻¹. The specific surface areas and porous nature of materials were further investigated by nitrogen adsorption/desorption measurements on nova 2200e XPS was analyzed by using a Thermo Scientific K-alpha surface analysis instrument.

Electrode preparation

The electrochemical properties of the samples were investigated with cyclic voltammetry (CV), Galvanostatic charge/discharge analysis, and impedance tests by using software-controlled conventional three electrode electrochemical cell (CHI 660C electrochemical workstation), consisting of the glassy carbon electrode (GCE) as the working electrode (WE), Ag/AgCl as the reference electrode, and the platinum wire as the counter electrode. The working electrode was prepared by mixing active material, carbon black, and polyvinylidene fluoride (PVDF) in 10% solution of *N*-methyl-2-pyrrolidone with a mass ratio of 75:20:5. Then, the prepared slurry was coating on Ni foil (1 cm × 1 cm) and dried at 80 °C for overnight. The mass of the electrode material is 0.8 mg. All the electrochemical measurements were performed in a 2-M KOH aqueous electrolyte solution at room temperature. The CV measurements were performed at scan rate of 10, 50, and 100 mV s⁻¹. A potential window in the range from -0.4 to 0.2 V was used in all the measurements.

Results and discussion

TGA analysis

Thermal properties of nanocomposites were determined by thermogravimetric analysis. The TGA spectra of pure and Fe₂O₃/G nanocomposite samples are shown in Fig. 1. The TGA curve of the composite displays a significant loss of

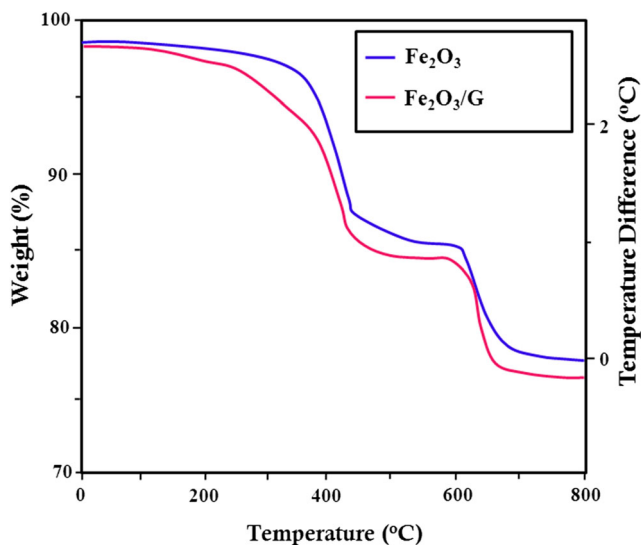


Fig. 1 TGA curve of pure and $\text{Fe}_2\text{O}_3/\text{G}$ nanocomposite samples

weight at approximately 250 °C. As can be seen from it, the weight loss over the temperature range up to 200 °C is about 1%. This might be due to the loss of residual water in the sample. The major weight loss between 350 and 450 °C is about 30%, which represents the amount of graphene [16]. The second weight loss was observed around 600 °C (4.5%) which could result from detachment of oxygen installed on graphene surface. The total weight loss was about 70–73%, and then the remaining material is composed of Fe_2O_3 only. This TG analysis confirms again the formation of Fe_2O_3 as the product of the deposition.

XRD analysis

X-ray diffraction is used to identify its structure and average grain size of the samples. Figure 2 shows the powder XRD pattern of pure GO, Fe_2O_3 , and $\text{Fe}_2\text{O}_3/\text{G}$ nanocomposite. In pure graphene, the broad peak in range of 20–30° is corresponded to the (002) diffraction of graphene. It can be seen that all the diffraction peaks could be readily indexed as a pure rhombohedral phase of $\alpha\text{-Fe}_2\text{O}_3$ (hematite, space group: R3c) with lattice constants $a = 0.511 \text{ \AA}$ and $c = 0.1321 \text{ \AA}$, which are in good agreement with the values given in the standard card (JCPDS no. 33–0664). Moreover, no other impurities were detected, which suggests the high purity of the as-prepared product. At the same time, characteristic diffraction peaks of Fe_2O_3 are also revealed in the XRD pattern of $\text{Fe}_2\text{O}_3/\text{graphene}$ composite, demonstrating the formation of Fe_2O_3 on surface of graphene. [17]. Compared to pure Fe_2O_3 , diffraction peaks of $\text{Fe}_2\text{O}_3/\text{G}$ composite are relatively broad, indicating that the crystals constituting the products are of small sizes. The average crystalline sizes of the pure and $\text{Fe}_2\text{O}_3/\text{G}$ nanocomposite

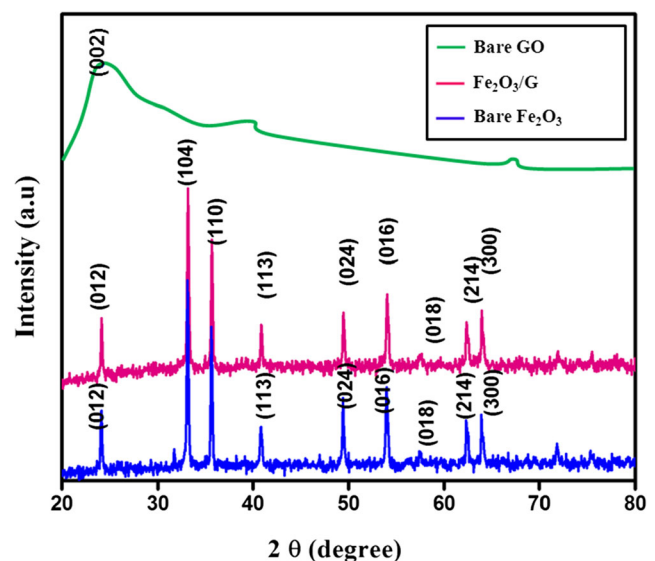


Fig. 2 Powder XRD pattern of pure GO, Fe_2O_3 , and $\text{Fe}_2\text{O}_3/\text{G}$ nanocomposite samples

electrodes were calculated by using Scherrer's equation [18].

$$d = \frac{K\lambda}{\beta \cos\theta}$$

where d is the mean crystallite size, K is the shape factor taken as 0.89, λ is the wavelength of the incident beam, β is the full width at half maximum, and θ is the Bragg angle. The average crystalline size was calculated as 35 nm and 25 nm for pure and $\text{Fe}_2\text{O}_3/\text{G}$ nanocomposite respectively.

TEM and EDS analysis

The morphology, particle size, and crystallinity of the samples have been investigated from TEM images. Figure 3a shows the TEM image of pure graphene; it consists of nanosheet with transparent and wrinkle. Figure 3c, d shows the TEM images of pure and $\text{Fe}_2\text{O}_3/\text{G}$ nanocomposite samples respectively. It was clear evidence that both the samples showed mainly spherical nanoparticles with homogeneously anchored to the graphenes with uniform sizes less than 35 nm. Enlarged HRTEM image of Fe_2O_3 (Fig. 3c) clearly indicates the high-quality crystalline character of $\alpha\text{-Fe}_2\text{O}_3$. The measured distinct spacing of periodic lattice fringes is 0.24 nm, assigned to the interspacing of (110) planes of hematite $\alpha\text{-Fe}_2\text{O}_3$, exactly matching with the XRD results. In order to confirm the chemical composition of the samples, EDAX measurement was carried out. Figure 3e, f shows the TEM-based EDAX spectra of pure and $\text{Fe}_2\text{O}_3/\text{G}$ nanocomposite sample. In pure graphene, the result shows the presence of C (65.38 at Wt%) and O (34.62 at Wt%) peaks, whereas in $\text{Fe}_2\text{O}_3/\text{G}$ composite, the samples mainly composed of Fe, C, and O elements,

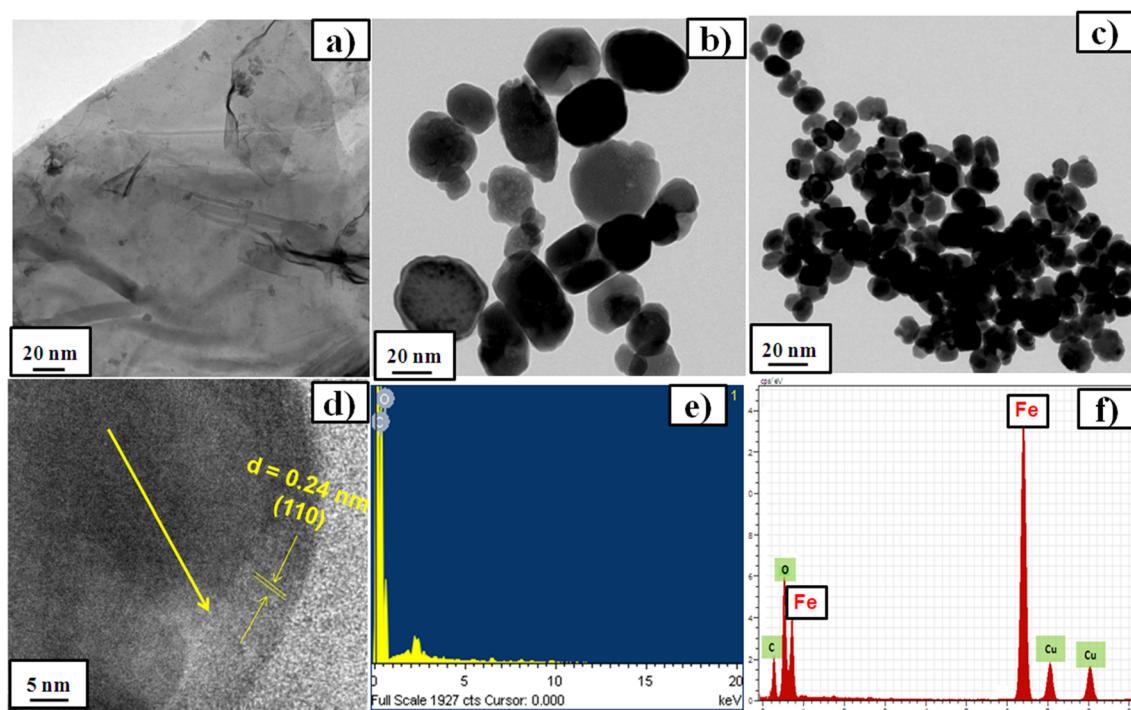


Fig. 3 TEM images of **a** pure graphene, **b** Fe_2O_3 , **c** $\text{Fe}_2\text{O}_3/\text{G}$ nanocomposite, **d** HRTEM image of Fe_2O_3 , **e** EDS analysis of pure GO, and **f** $\text{Fe}_2\text{O}_3/\text{G}$ nanocomposites

which confirm the purity of the samples. The Cu element was found in the composition, due to the grid used for EDS measurements. The weight percentages of graphene were estimated to be 58.42 wt% for Fe_2O_3 –graphene composite. This value is slightly less than the theoretical value (66.7 wt%), which is calculated based on the experimental conditions.

Raman spectra analysis

Raman spectroscopy can be used to gain information about the structural changes in carbonaceous materials. The Raman spectra of pure and $\text{Fe}_2\text{O}_3/\text{G}$ nanocomposite samples were shown in Fig. 4. It was noted that the fundamental Raman scattering peaks for Fe_2O_3 are observed at 221, 282, 379, and 496 cm^{-1} corresponding to the $\text{A}_{\text{g}}(1)$, $\text{E}_{\text{g}2} + \text{E}_{\text{g}3}$, $\text{E}_{\text{g}4}$, and $\text{A}_{1\text{g}}(2)$ modes [19], respectively. In the case of $\text{Fe}_2\text{O}_3/\text{G}$ composite, in addition to the bands corresponding to Fe_2O_3 , the characteristic D and G bands of graphene also appear clearly, respectively. These results further suggest the good integration of graphene and Fe_2O_3 nanoparticles.

XPS analysis

XPS measurements were employed to further characterize the elemental components of the pure Fe_2O_3 and $\text{Fe}_2\text{O}_3/\text{G}$ nanocomposites. The XPS survey spectrum was carried out for bare Fe_2O_3 and $\text{Fe}_2\text{O}_3/\text{G}$ composite and depicts in Fig. 5a along with the core level spectra of Fe 2p, O 1s, and C 1s

peaks that are shown in Fig. 5b–d, respectively. In the magnified spectrum for pure Fe_2O_3 (Fig. 5b), the binding energies of $\text{Fe}2\text{p}_{1/2}$ and $\text{Fe}2\text{p}_{3/2}$ are 725.1 and 711.8 eV, respectively, whereas in $\text{Fe}_2\text{O}_3/\text{G}$ nanocomposite, two peaks that appeared at 726.3 eV and 713.23 eV are exhibited in the Fe 2p spectrum (Fig. 5b), which correspond to the $\text{Fe} 2\text{p}_{1/2}$ and $\text{Fe} 2\text{p}_{3/2}$ spin-orbit peaks of Fe_2O_3 [20]. The O 1s peak of pure Fe_2O_3 is observed at 530.5 eV and for $\text{Fe}_2\text{O}_3/\text{G}$ nanocomposite; the peak that appeared at 531.1 eV in the O 1s spectra corresponds

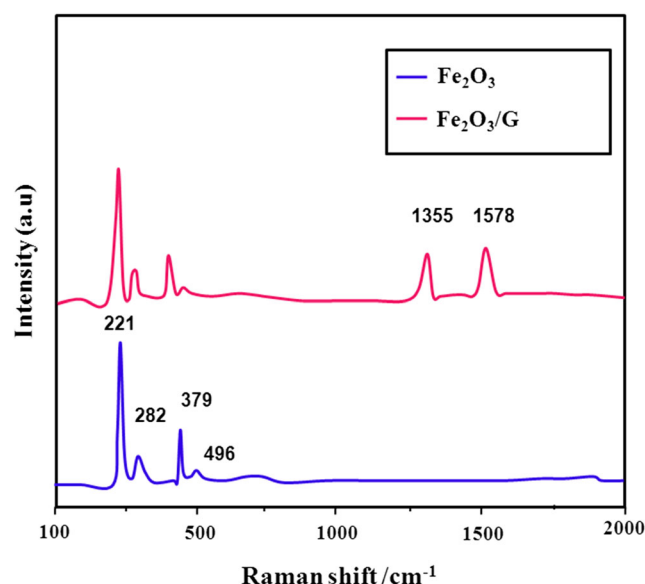


Fig. 4 Raman spectra of pure and $\text{Fe}_2\text{O}_3/\text{G}$ nanocomposite samples

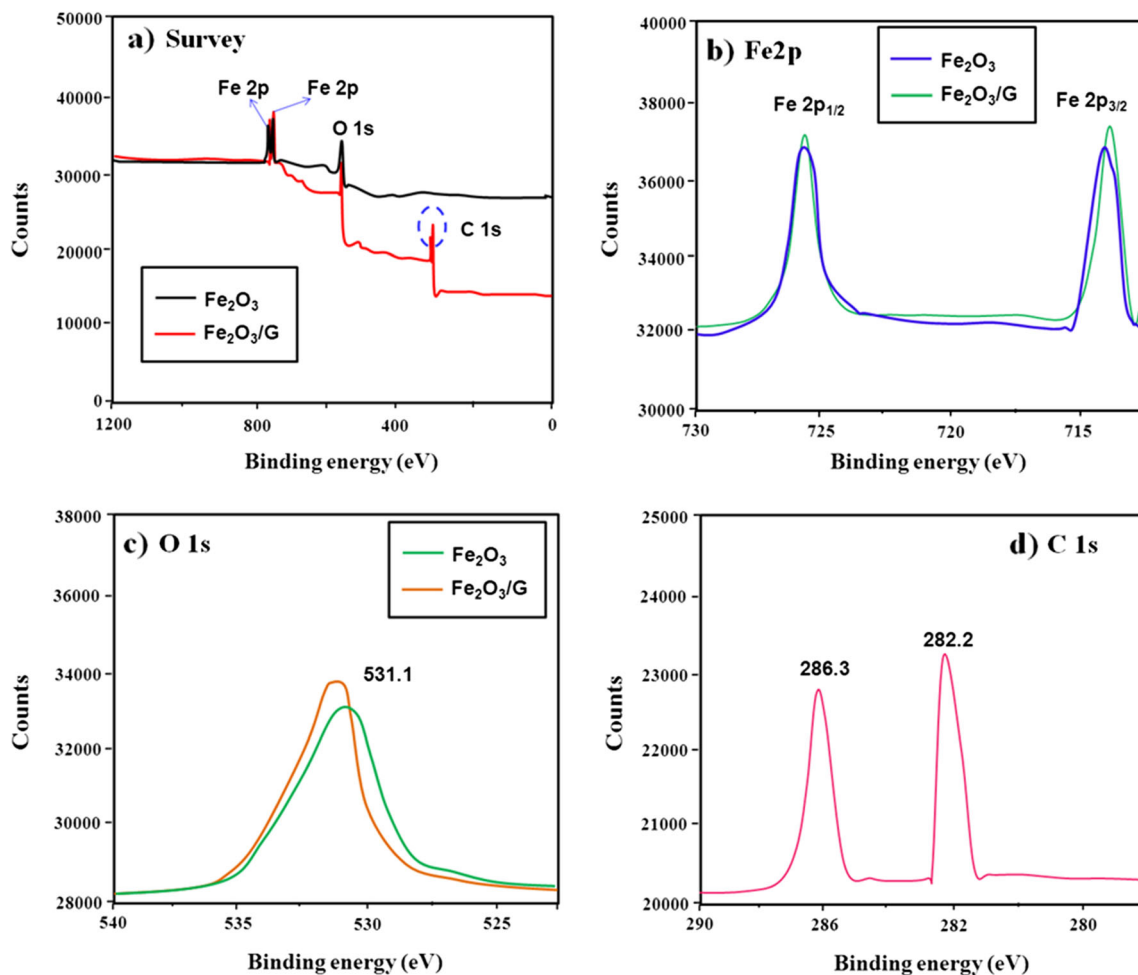


Fig. 5 a The full-range XPS survey spectrum of Fe₂O₃ and Fe₂O₃/G and the high-resolution spectrum of b Fe 2p, c O 1s, and d C 1s (Fe₂O₃/G nanocomposite)

to the oxygen species in the metal oxide (Fig. 5c). In the C 1s spectrum (Fig. 5d), the peaks at 282.2 and 286.3 eV belong to the sp²-C and sp³-C bonds of rGO, respectively. XPS results again supported that successful loading of Fe₂O₃ nanoparticles in the graphene surface.

BET surface analysis

The specific surface area and pore size distribution are the important factors that can intensely show the performance of the electrodes. The surface area of the samples was analyzed by using Brunauer–Emmett–Teller (BET). From the N₂ adsorption–desorption isotherm (Fig. 6a), it is observed that both the samples exhibit an irreversible type IV isotherm in the Brunauer classification that corresponds to the typical mesoporous feature. The specific BET surface area was found to be 76 and 91 m² g^{−1} for pure and Fe₂O₃/G nanocomposite electrodes respectively. The resulting increase in surface area of Fe₂O₃/G than Fe₂O₃ clearly endorses the TEM and XRD analysis results. The corresponding BJH pore size distribution of

the samples is shown in Fig. 6b and found to be 10 and 17 nm for pure and Fe₂O₃/G nanocomposite electrodes respectively.

Electrochemical analysis

CV analysis

CV and galvanostatic charge–discharge measurements were examined in a half-cell configuration with three electrode mode to evaluate the electrochemical properties of the Fe₂O₃–graphene composites. Figure 7a, b shows the representative CV curves of the Fe₂O₃ and Fe₂O₃/G composite electrodes at different scan rates in 2 M KOH electrolyte with a potential window between −0.4 and 0.2 V (vs. Ag/AgCl). The curve shape of both samples that showed shapes are obviously not rectangular, indicating pseudocapacitive character. Moreover, the shape of the CV curves was retained even at the very high scan rate of 100 mV s^{−1}. At an even higher scan rate of 100 mV s^{−1}, the rectangularity of the CV deteriorated

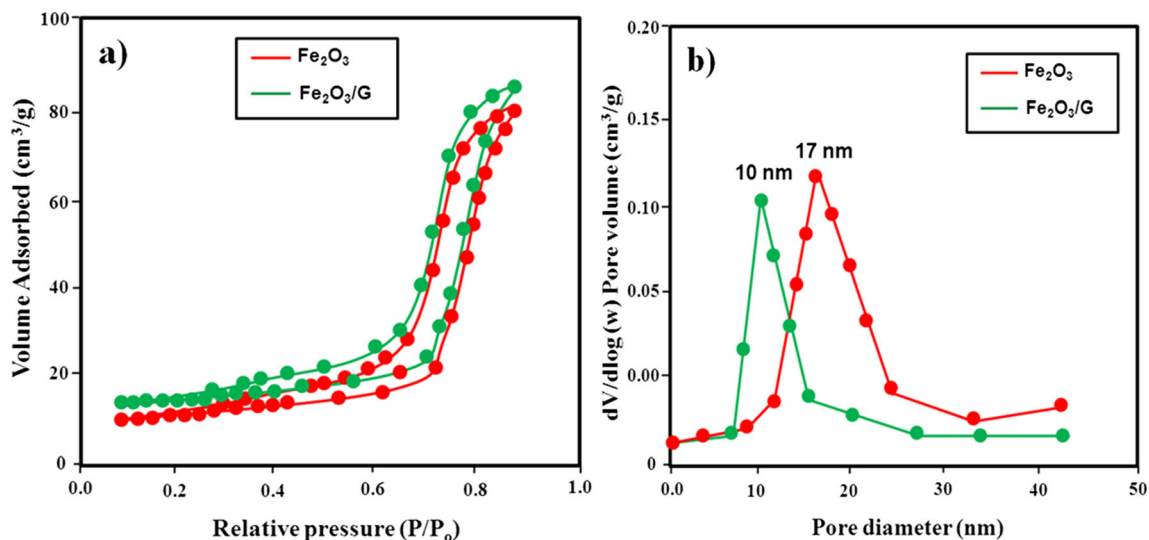


Fig. 6 **a** N_2 nitrogen adsorption and desorption and **b** pore size distribution spectra of pure and Fe_2O_3/G nanocomposite samples

but was still logically good. The results suggest that Fe_2O_3/G electrode is a tremendous electrochemical reversibility, negligible internal resistance, and uniform working potential. This could be due to high charge transport/transfer rates and uniform distribution of Fe_2O_3/G nanocomposite electrodes achieved by using the graphene. The excellent rate capability of the electrode can be further investigated by the galvanostatic charging/discharging analysis at different current densities.

Galvanostatic charge/discharge analysis

Figure 8a, b shows the charge–discharge behavior of the as-prepared Fe_2O_3 and Fe_2O_3/G electrodes at different current densities in 2 M KOH electrolyte with a potential window between -0.4 and 0.2 V (vs. Ag/AgCl). The specific capacitance value of all of the electrode materials

was again determined from charge/discharge profiles by using the following equation [21].

$$C_s = \frac{i\Delta t}{m\Delta V} \quad (1)$$

where C_s is the specific capacitance ($F\ g^{-1}$), I is the specific current (A), Δt is the discharge time (s), m is the mass of the active material (g), and ΔV is the potential window (V). The discharge specific capacitance of the $Fe_2O_3/graphene$ electrodes at the current density of $2\ A\ g^{-1}$ is $315\ F\ g^{-1}$, which is higher than the already reported literature values [22]. The detailed specific capacitance value of both Fe_2O_3 and Fe_2O_3/G composites is shown in Table 1. The variation of specific capacitance as a function of different current density is also shown in Fig. 8c, d. Moreover, the galvanostatic charge discharge (GCD) results demonstrate that Fe_2O_3/G composite shows a specific capacitance as high as $315\ F\ g^{-1}$ at a discharge current density of $2\ A\ g^{-1}$. Even at the current density of $10\ A\ g^{-1}$, the specific

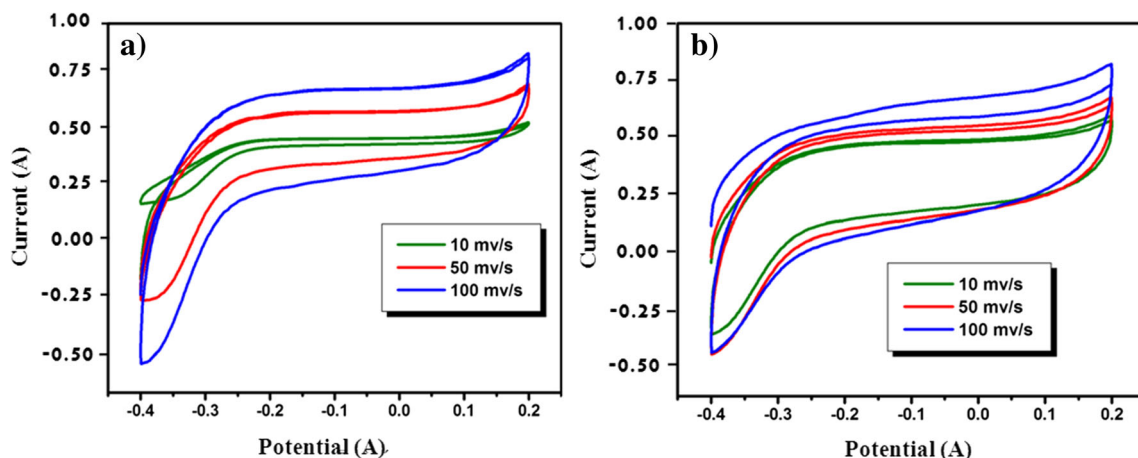
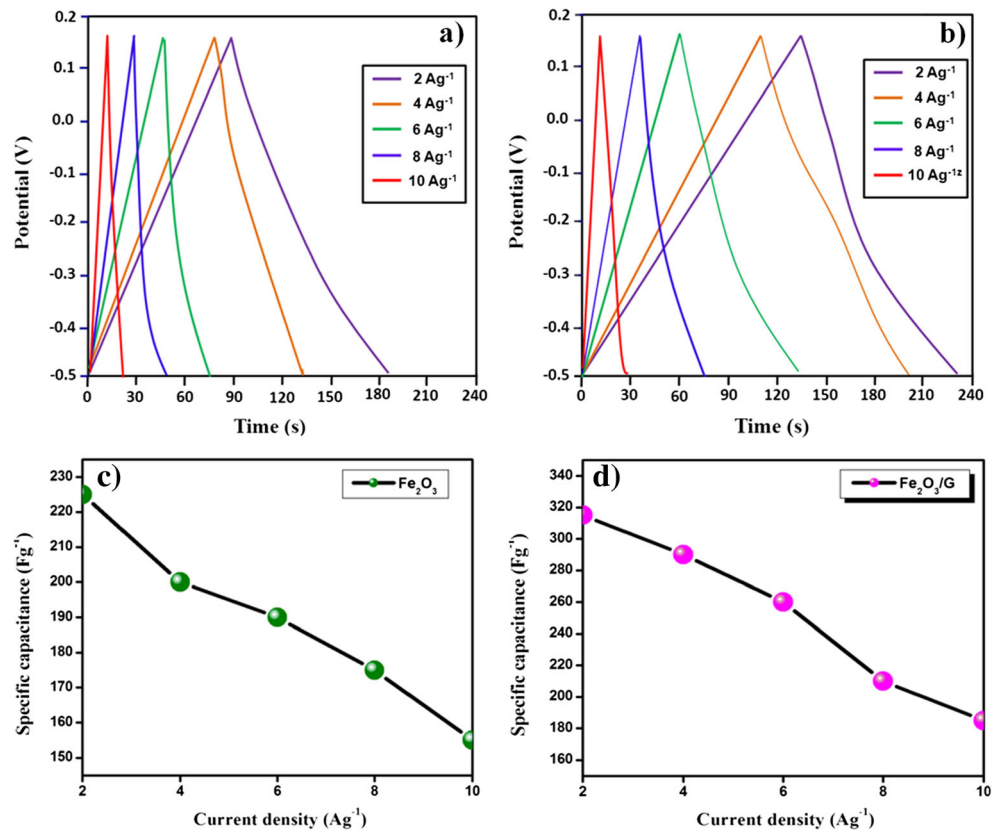


Fig. 7 CV curve of **a** Fe_2O_3 and **b** Fe_2O_3/G nanocomposite with different scan rates

Fig. 8 Charge–discharge behavior of **a** Fe₂O₃ and **b** Fe₂O₃/G electrodes at different current densities and **c**, **d** variation-specific capacitance values as a function current density



capacitance is still as high as 185 F g⁻¹. The remarkably increased capacitance of Fe₂O₃/G may be caused by the combination of electric double-layer capacitance of G and faradic pseudocapacitance of Fe₂O₃. The decrease in specific capacitance with the increase of current densities (2 to 10 A g⁻¹) is attributed to the relatively insufficient faradaic redox reaction of the active materials under higher discharge current densities.

Cyclability test

The cycle life is another important factor for the supercapacitor materials. The electrochemical cycle stability of the as-prepared Fe₂O₃ and Fe₂O₃/G electrodes was

evaluated at a current density of 2 A g⁻¹ for 2000 cycles as shown in Fig. 9a, b and inset. The inset shows the last 500 cycles of the electrodes. As shown in Fig. 9a, b, the capacitance retention rate of the composite electrode remained at a very high value of 98%, after 2000 cycles, revealing the excellent electrochemical stability of the Fe₂O₃/G electrode, while that of the α-Fe₂O₃ electrode dropped to 88%. The excellent capacitive performance of the Fe₂O₃/G composite electrode is probably attributed to the constructive synergistic effects between the Fe₂O₃ and graphene. Graphene also provides a highly conductive network for electron transport during the charge and discharge processes, thus reducing the polarization of the electrodes, which results in enhance the electrochemical

Table 1 Summary of recent reports of Fe₂O₃/G-based material for supercapacitors

Synthesis route	Surface area (m ² g ⁻¹)	Pore volume (cm ³ g ⁻¹)	Specific capacitance (F g ⁻¹)	Electrolyte	Ref
SILAR	NA	NA	178	1 M NaOH	[23]
Wet chemical synthesis	138.4	0.32	240	1 M H ₃ PO ₄	[24]
SILAR	85.4	0.4	283	1 M NaOH	[25]
Electrospinning	56	0.087	256	1 M LiOH	[26]
Solvent deficient	40	0.089	258	1 M KOH	[27]
Hydrothermal	91	0.10	315	2 M KOH This work	

NA not available

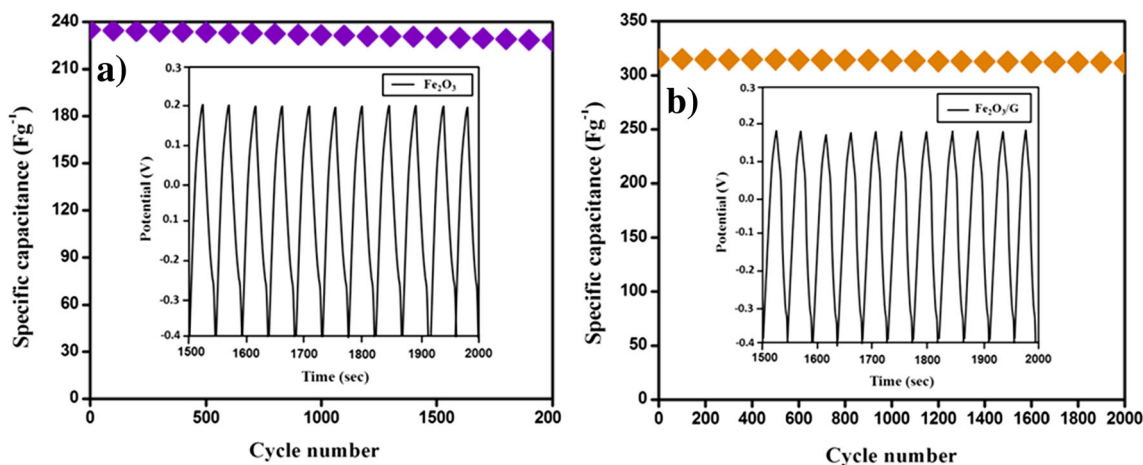


Fig. 9 Cycling stability of the electrodes for 2000 cycles at a current density of 2 A g^{-1} . Bottom inset is the charge–discharge curves of the last 500 cycles. **a** Fe_2O_3 . **b** $\text{Fe}_2\text{O}_3/\text{G}$

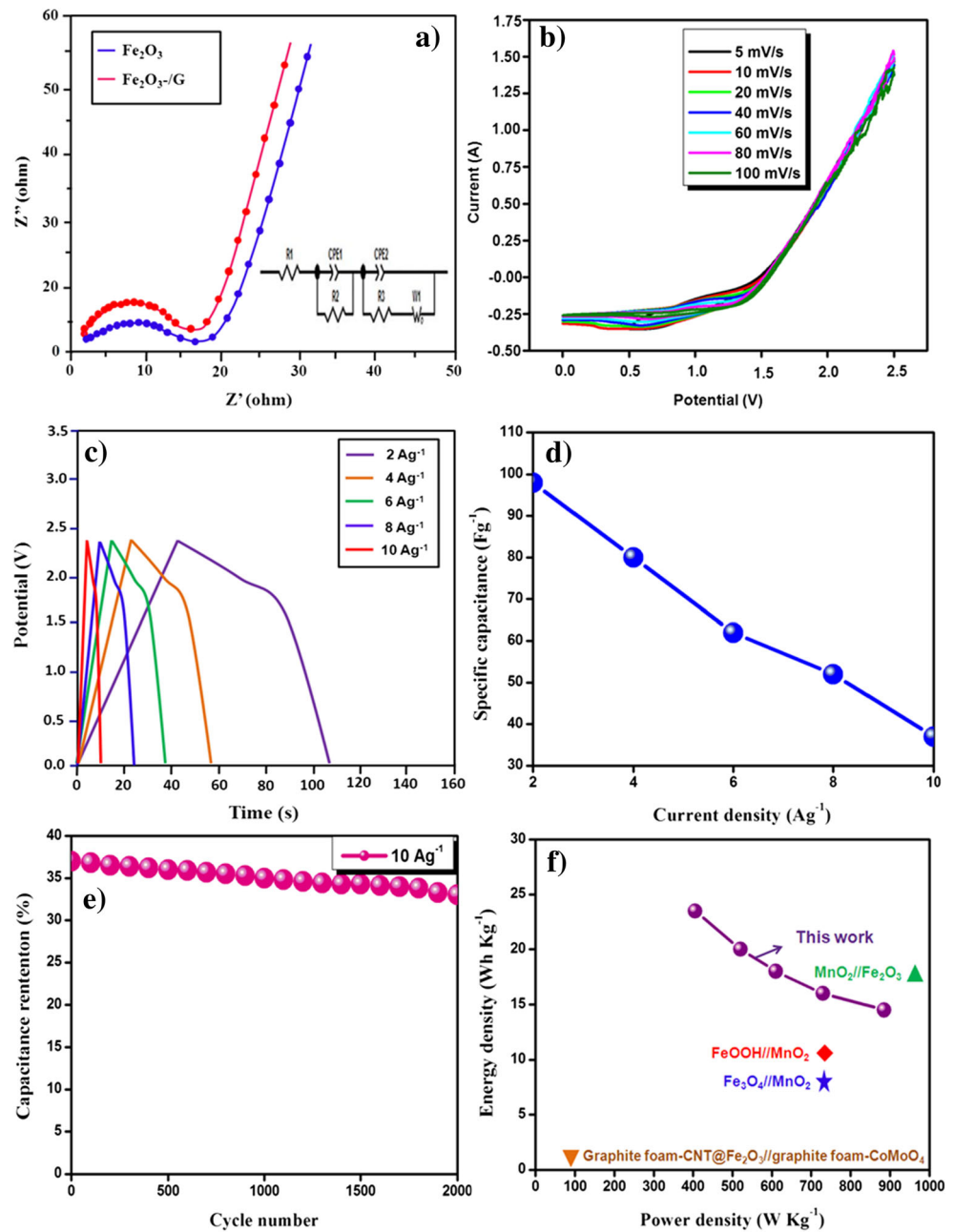
performance of Fe_2O_3 [28]. According to the specific capacitance of the supercapacitors, the energy density (E , in W h kg^{-1}) and power density (P , in W kg^{-1}) could be further calculated using the equations, $E = 1/2CU^2$ and $P = E/t$, respectively [29]. Moreover, the proposed electrodes showed superior electrochemical performance than that of previous reports and shown in Table 1 [23–27]. The overall electrochemical results suggest that $\text{Fe}_2\text{O}_3/\text{G}$ is superior electrochemical performance than pure Fe_2O_3 . This could be due to the existence of Fe_2O_3 nanoparticles and graphene sheets that enables fast electronic and ionic transport through the active materials to charge collector and make the charge–transfer resistance of $\text{Fe}_2\text{O}_3/\text{G}$ electrode decrease and thus improve the electrochemical performance, which results in specific capacitance of the $\text{Fe}_2\text{O}_3/\text{graphene}$ electrodes at the current density of 2 A g^{-1} is 315 F g^{-1} . Moreover, Fe_2O_3 nanoparticles on the surface of graphene sheets can act as spacers to efficiently prevent the aggregation of the nanoparticles as well as the restacking of graphene sheets, avoiding/weakening the loss of their high active surface area. Moreover, the large specific surface area could significantly improve the electrochemical reactive sites and better penetration of the electrolyte in to the whole electrode materials, which will generate the high supercapacitive performance.

EIS tests

Complementary to CV and galvanostatic charge/discharge measurements, EIS provides useful information on the electrochemical frequency of a system for the measurement of redox reaction resistance. For further understanding, the impedance of Fe_2O_3 and $\text{Fe}_2\text{O}_3/\text{G}$ composite electrodes was measured in the frequency range of $100\text{--}0.1 \text{ kHz}$ at open circuit. Figure 10a shows the Nyquist plots of Fe_2O_3 and $\text{Fe}_2\text{O}_3/\text{G}$ electrodes. It can be seen that both the electrode exhibited a vertical capacitive line in the low-frequency region, semicircle in the high-

frequency region and a straight line inclined at a constant phase in the mid-frequency region. The high-frequency semicircle region is due to the charge transfer reaction at the interface of the electrolyte/oxide electrode, and it corresponds to the charge transfer resistance (R_{ct}) [30]. It is clear proof that the R_{ct} of $\text{Fe}_2\text{O}_3/\text{G}$ (2.01Ω) is smaller than that of Fe_2O_3 (2.43Ω), indicating that the electrochemical reaction on the electrode/electrolyte interface is the more facile for $\text{Fe}_2\text{O}_3/\text{G}$. This confirms that the formation of Fe_2O_3 nanoparticles really makes the electronic resistance of the electrode decrease. These results prove that the formation of Fe_2O_3 nanoparticles on G can significantly improve the electrical performance due to the intrinsic resistance change of the active material and less aggregation of the graphene. To further evaluate the $\text{Fe}_2\text{O}_3/\text{G}$ electrode for practical applications, an asymmetric supercapacitor was manufactured by using $\text{Fe}_2\text{O}_3/\text{G}$ as the positive electrode and AC as the negative electrode. Figure 10b shows CV curves of the $\text{Fe}_2\text{O}_3/\text{G}@\text{AC}$ asymmetric device performed at different scanning rates ranging from 5 to 100 mV s^{-1} . It can be seen that the potential range could be max to 2 V , and all CV curves exhibited redox peaks, revealing the combined contribution of both EDLC and battery-type electrodes on the total CV behaviors. The GCD curves at different current densities are shown in Fig. 10c, and the shapes of all curves are triangular, further confirming excellent capacitive performance of the $\text{Fe}_2\text{O}_3/\text{G}@\text{AC}$ asymmetric device. As shown in Fig. 10d, the specific capacitance of the $\text{Fe}_2\text{O}_3/\text{G}@\text{AC}$ ASC is calculated from GCD curve and a maximum capacitance of 98 F g^{-1} at a discharge current density of 2 A g^{-1} . The cyclic durability of the $\text{Fe}_2\text{O}_3/\text{G}@\text{AC}$ ASC is further evaluated at 10 A g^{-1} for 2000 cycles, and it can be seen that the ASCs retains 88% of the initial capacitance, proving its good cycling performance (Fig. 10e). Further, two important electrochemical parameters like power density and energy density are measured to get the information about energy storage performance of supercapacitors. The plot consisting of energy

Fig. 10 **a** Nyquist plots of Fe₂O₃ and Fe₂O₃/G electrodes with a frequent range of 0.1 Hz–100 kHz in 1 M KOH electrolyte and equivalent circuit (inset). **b** CV curves at different scan rates. **c** GCD curves at various current densities. **d** Variation of specific capacitance with different current densities. **e** Cycling stability of the Fe₂O₃/G//AC device for 2000 cycles at the current density of 10 A g⁻¹. **f** Ragone plots



density and power density is presented in Fig. 10f. The energy density (W h kg⁻¹) and power density (kW kg⁻¹) are calculated by using the equations reported literature [31]. The results show high-energy density of 23.5 W h kg⁻¹ at a power density of 405 W kg⁻¹. Even at high power density of 885 W kg⁻¹, relative high-energy densities of 14.5 W h kg⁻¹ are achieved. The values of energy and power densities obtained in the present work are higher than compared with some reported similar Fe₂O₃, such as FeOOH//MnO₂ (12 W h kg⁻¹) [32], Fe₃O₄//MnO₂ (8 W h kg⁻¹) [33], MnO₂//Fe₂O₃ (19.4 W h kg⁻¹) [34], and graphite foam-CNT@Fe₂O₃//graphite foam-CoMoO₄ (1.4 W h kg⁻¹) [35].

Conclusions

In summary, we have successfully developed a facile and one-step hydrothermal method for the synthesis of pure and α-Fe₂O₃/G nanocomposite, which can be scaled up in a large quantity. XRD, TEM, Raman, and XPS analyses confirm that well-crystalline Fe₂O₃ nanoparticles in rhombohedral phase of α-Fe₂O₃ (hematite, space group: R3c) with 25–35 nm in size are highly encapsulated in a graphene matrix. The electrochemical property of Fe₂O₃ was significantly improved by graphene matrix. The Fe₂O₃/G nanocomposite electrode shows a specific capacitance of 315 F g⁻¹ at a current density

of 2 A g^{-1} and results in good long-term cyclic stability 98% capacitance retention after 2000 cycles. This material takes the advantage both of the electrical double layer capacitor from G and pseudocapacitance of Fe_2O_3 nanoparticles. Hence, the present $\alpha\text{-Fe}_2\text{O}_3/\text{G}$ nanocomposite electrodes proved to be an excellent anode material for fabrication of neutral aqueous asymmetric supercapacitors.

Compliance with ethical standards

Conflict of interest The authors declare that there is no conflict of interest.

Publisher's note Springer Nature remains neutral with regard to jurisdictional claims in published maps and institutional affiliations.

References

- Jing X, Wang Q, Wang X, Xiang Q, Bo L, Di C, Shen G (2013) Flexible asymmetric supercapacitors based upon Co_9S_8 nanorod// Co_3O_4 @ RuO_2 nanosheet arrays on carbon cloth. *ACS Nano* 7: 5453–5462
- Fan L-Q, Liu G-J, Zhang C-Y, Ji-Huai W, Wei Y-L (2015) Facile one-step hydrothermal preparation of molybdenum disulfide/carbon composite for use in supercapacitor. *Int J Hydrog Energy* 40:10150–10157
- Tang Y, Chen T, Yu S, Qiao Y, Shichun M, Hu J, Gao F (2015) Synthesis of graphene oxide anchored porous manganese sulfide nanocrystals via the nanoscale Kirkendall effect for supercapacitors. *J Mater Chem A* 3:12913–12919
- Xiang D, Yin L, Wang C, Zhang L (2016) High electrochemical performance of $\text{RuO}_2\text{-Fe}_2\text{O}_3$ nanoparticles embedded ordered mesoporous carbon as a supercapacitor electrode material. *Energy* 106:103–111
- Peng X, Peng L, Wu C, Xie Y (2014) Two dimensional nanomaterials for flexible supercapacitors. *Chem Soc Rev* 43: 3303–3323
- Shivakumara S, Penki TR, Munichandraiah N (2014) High specific surface area $\alpha\text{-Fe}_2\text{O}_3$ nanostructures as high performance electrode material for supercapacitors. *Mater Lett* 131:100–103
- Lin F, Li X, Zhao Y, Yang Z (2016) Control strategies with dynamic threshold adjustment for supercapacitor energy storage system considering the train and substation characteristics in urban rail transit. *Energies* 9:257
- Subramanian V, Hall SC, Smith PH, Rambabu B (2004) Mesoporous anhydrous RuO_2 as a supercapacitor electrode material. *Solid State Ionics* 175:511–515
- Patil UM, Kulkarni SB, Jamadade VS, Lokhande CD (2011) Chemically synthesized hydrous RuO_2 thin films for supercapacitor application. *J Alloys Compd* 509:1677–1682
- Liu T, Pell WG, Conway BE (1997) Self-discharge and potential recovery phenomena at thermally and electrochemically prepared RuO_2 supercapacitor electrodes. *Electrochim Acta* 42:3541–3552
- Qu QT, Yang SB, Feng XL (2011) 2D sandwich-like sheets of Iron oxide grown on graphene as high energy anode material for supercapacitors. *Adv Mater* 23:5574–5580
- Zhang H, Zhang X, Lin H, Wang K, Sun X, Xu N, Li C, Ma Y (2015) Graphene and maghemite composites based supercapacitors delivering high volumetric capacitance and extraordinary cycling stability. *Electrochim Acta* 156:70–76
- Singh V, Joung D, Zhai L, Das S, Khondaker S, Seal S (2011) Graphene based materials: past, present and future. *Prog Mater Sci* 56:1178–1271
- Wang D, Li Y, Wang Q, Wang T (2012) Nanostructured Fe_2O_3 -graphene composite as a novel electrode material for supercapacitors. *J Solid State Electrochem* 16:2095–2102
- Zhang H, Gao Q, Yang K, Tan Y, Tian W, Zhu L, Li Z, Yang C (2015) Solvothermally induced $\alpha\text{-Fe}_2\text{O}_3$ /graphene nanocomposites with ultrahigh capacitance and excellent rate capability for supercapacitors. *J Mater Chem A* 3:22005–22011
- Tian LL, Zhuang QC, Li J, Wu C, Shi YL, Sun SG (2012) The production of self-assembled Fe_2O_3 -graphene hybrid materials by a hydrothermal process for improved Li-cycling. *Electrochim Acta* 65:153–158
- Zhu XJ, Zhu W, Murali YS, Stollers MD, Ruoff RS (2011) Nanostructured reduced graphene oxide/ Fe_2O_3 composite as a high-performance anode material for lithium ion batteries. *ACS Nano* 5:3333–3338
- Parthibavarman M, Vallalperuman K, Sathishkumar S, Durairaj M, Thavamani K (2014) A novel microwave synthesis of nanocrystalline SnO_2 and its structural optical and dielectric properties. *J Mater Sci Mater Electron* 25:730–735
- Lee KK, Deng S, Fan HM, Mhaisalkar S, Tan HR, Tok ES, Loh KP, Chin WS, Sow CH (2012) $\alpha\text{-Fe}_2\text{O}_3$ nanotubes-reduced graphene oxide composites as synergistic electrochemical capacitor materials. *Nanoscale* 4:2958–2961
- Zhang H, Xie AJ, Wang CP, Wang HS, Shen YH, Tian XY (2013) Novel rGO/ $\alpha\text{-Fe}_2\text{O}_3$ composite hydrogel: synthesis, characterization and high performance of electromagnetic wave absorption. *J Mater Chem A* 1:8547–8552
- Karthik M, Parthibavarman M, Kumaresan A, Prabhakaran S, Hariharan V, Poonguzhali R, Sathishkumar S (2017) One-step microwave synthesis of pure and Mn doped WO_3 nanoparticles and its structural, optical and electrochemical properties. *J Mater Sci Mater Electron* 28:6635–6642
- Wang D-W, Li Y-Q, Wang Q-H, Wang T-M (2012) Nanostructured Fe_2O_3 -graphene composite as a novel electrode material for supercapacitors. *J Solid State Electrochem* 16:2095–2102
- Kore RM, Lokhande BJ (2017) A robust solvent deficient route synthesis of mesoporous Fe_2O_3 nanoparticles as supercapacitor electrode material with improved capacitive performance. *J Alloys Compd* 725:129–138
- Chaudhari S, Bhattacharjya D, Yu JS (2013) 1-Dimensional porous $\alpha\text{-Fe}_2\text{O}_3$ nanorods as high performance electrode material for supercapacitors. *RSC Adv* 3:25120–25128
- Gund GS, Dubal DP, Chodankar NR, Cho JY, Romero PG, Park C, Lokhande CD (2015) Low cost flexible supercapacitors with high energy density based on nanostructured MnO_2 and Fe_2O_3 thin films directly fabricated onto stainless steel. *Sci Rep* 5:2454
- Binitha G, Soumya MS, Madhavan AA, Praveen P, Balakrishnan A, Subramanian KRV, Reddy MV, Nair SV, Nair AS, Sivakumar N (2013) Electrospun $\alpha\text{-Fe}_2\text{O}_3$ nanostructures for supercapacitor applications. *J Mater Chem A* 1:11698–11704
- Kulal PM, Dubal DP, Lokhande CD, Fulari VJ (2011) Chemical synthesis of Fe_2O_3 thin films for supercapacitor application. *J Alloys Compd* 509:2567–2571
- Wang B, Park J, Wang CY, Ahn H, Wang GX (2010) Mn_3O_4 nanoparticles embedded into graphene nanosheets: preparation, characterization, and electrochemical properties for supercapacitors. *Electrochim Acta* 55:6812–6817
- Zhang Y, Xu J, Zheng Y, Zhang Y, Hu X, Xu T (2017) Construction of CuCo_2O_4 @ CuCo_2O_4 hierarchical nanowire arrays grown on Ni foam for high performance supercapacitors. *RSC Adv* 7:3983–3991

30. Wang Y, Shi Z-Q, Huang Y, Ma Y-F, Wang C-Y, Chen M-M, Chen Y-S (2009) Supercapacitor devices based on graphene materials. *J Phys Chem C* 113:13103–13107
31. Yang H, Kannappan S, Pandian AS, Jang JH, Lee YS, Lu W (2017) Graphene supercapacitor with both high power and energy density. *Nanotechnology* 28:445401
32. Jin WH, Cao GT, Sun JY (2008) Hybrid supercapacitor based on MnO₂ and columned FeOOH using Li₂SO₄ electrolyte solution. *J Power Sources* 175:686–691
33. Cottineau T, Toupin M, Delahaye T, Brousse T, Belanger D (2006) Nanostructured transition metal oxides for aqueous hybrid electrochemical supercapacitors. *Appl Phys A Mater Sci Process* 82:599–606
34. Gund GS, Dubal DP, Chodankar NR, Cho JY, Gomez-Romero P, Park C, Lokhande CD (2015) Low-cost flexible supercapacitors with high-energy density based on banostructured MnO₂ and Fe₂O₃ thin films directly fabricated onto stainless steel. *Sci Rep* 5: 12454
35. Guan C, Liu JL, Wang YD, Mao L, Fan ZX, Shen ZX, Zhang H, Wang J (2015) Iron oxide- decorated carbon for supercapacitor anodes with ultrahigh energy density and outstanding cycling stability. *ACS Nano* 9:5198–5207